Modeling Convective Heat Transfer with Graphite Foams

James Klett, April McMillan
Oak Ridge National Laboratory, Oak Ridge, TN, 37831

Background

In recent decades, many improvements in electronic components ranging from computer chips to power converters have driven the need for more efficient devices for transferring heat. Many techniques have been explored to improve efficiencies of heat transfer devices, such as micro-channels, heat pipes, and other exotic designs. One design efficiently utilizes metal foams to enhance heat transfer by increasing the surface area of heat transfer. These metal foams have a bulk apparent thermal conductivity at least an order of magnitude greater than traditional non-metallic foams (1). These metallic foams have been successfully used as heat exchangers for airborne equipment, compact heat sinks for power electronics, heat shields, and air-cooled condenser towers and regenerators (2, 3). There has been modeling efforts (1) to produce design parameters and constraints using these unique materials. However, the limitations of these metal foams are that since they are porous structures of their parent material, their overall conductivity is up to an order of magnitude less than their dense parent material. For example, (see Table 1) an aluminum foam that is 10% dense (90% open porous), can exhibit a bulk thermal conductivity of about 10 W/mK compared to 180 for the dense aluminum. For this reason, it is expected that foam made from a material with a higher ligament thermal conductivity than the metals should out perform the metal foams. Such a material exists in a newly developed foam: Thermally Conductive Graphite Foam (4-8).

Table 1.

	Relative Density [%]	Ligament Conductivity [W/m·K]	Bulk Conductivity [W/m·K]
Aluminum Foam	10	180	~10
Copper Foam	10	400	~25

Carbon foams were first developed by researchers in the late 60's as a reticulated vitreous (glassy) carbon foam. Ford (9) reported the first carbon foams made by converting existing thermosetting organic polymer foams to a carbonized foam through a simple heat treatment. Then, Googin et al. (10) at the Oak Ridge Atomic Energy Commission Laboratory reported the first process dedicated to controlling the structure and material properties of carbon and graphite foams by controlling the precursor material (see Figure 1). These foams were characterized by their excellent thermal insulation capabilities, with the graphite foams of Googin being stable thermal insulators up to temperatures as high as 2500C. Following the initial discoveries, many researchers in the 60's began exploring the variety of applications of these articles (11-20) ranging from electrodes to insulating articles for furnaces and other high temperature applications, up to 2500C. In fact, reticulated carbon foams (Figure 2) have even been used as the template for producing many of the metal and ceramic foams currently used in industry.

In the 1970's, research was focused primarily on producing carbon foams from alternative sources. For example, Klett, R. (16) at the Sandia National Laboratories produced the first carbon foams from a cork, a natural cellular precursor for foams made from cellulose. Others worked on many other processing and precursor changes in an attempt to either modify properties or reduce cost. However, all of these previous carbon foams were mainly used for thermal insulation (although some structural applications were found).

As the 90's began, researchers at the US Air Force Materials Lab pioneered research into mesophase derived graphitic foams specifically for replacing expensive 3-D woven fiber performs in polymer composites and replacements for honeycomb materials (21-23). Their work was centered around developing a highly structural material which was lightweight, and to date, exhibit the highest specific strength of carbon foams. In an attempt to produce very inexpensive carbon foams, researchers at West Virginia University developed a method to use coal as a precursor for high strength foams with excellent thermal insulation properties and high strengths. Then, in 1997, Klett, J. (24) at the Oak Ridge National Laboratory reported the first graphite foams with bulk thermal conductivities greater than 100 W/mK (recently, conductivites up to 180 W/mK have been reported (7, 8, 25)). At a thermal conductivity to weight ratio (κ/ρ) of greater than 200, compared to 45 for copper, and an open cellular structure; this graphite foam presented a unique solution to many heat transfer problems required by automotive and other energy related applications.

This material was different from the carbon and graphite foams produced previously. This material has a predominately spherical porosity with smaller openings between the cells (Figure 3). It is fabricated with the highly oriented sheets of the graphite parallel to the cell walls, yielding thermal conductivities in the ligaments as high as 1700 W/mK. At a relative density of approximately 0.3, this results in a bulk apparent thermal conductivity of more than 150 W/mK. Hence, a graphite foam can be produced with a bulk thermal conductivity almost equivalent to dense aluminum alloys, but at $1/5^{th}$ the weight. With this material being open celled, the potential for improved heat transfer has led to a frenzy of research on applications of this novel material ranging from automobile radiators to heat sinks for computer chips to leading edges with active cooling for spacecraft. However, one of the biggest limitations of this material to being utilized more readily is its lack of design parameters and basic understanding of the role of material properties on the heat transfer. Hence, this paper looks at the various design parameters and material variables as they relate to the potential heat transfer and attempts to give a better understanding on the use of the material in different applications as a heat transfer medium. Ashby et al. (1), provide an excellent review and development of a heat transfer model using reticulated metal foams. However, since the new graphite foams contain pores of different shape, size, and drastically different thermal conductivities, this model must be revisited in order to apply it to graphitic foams.

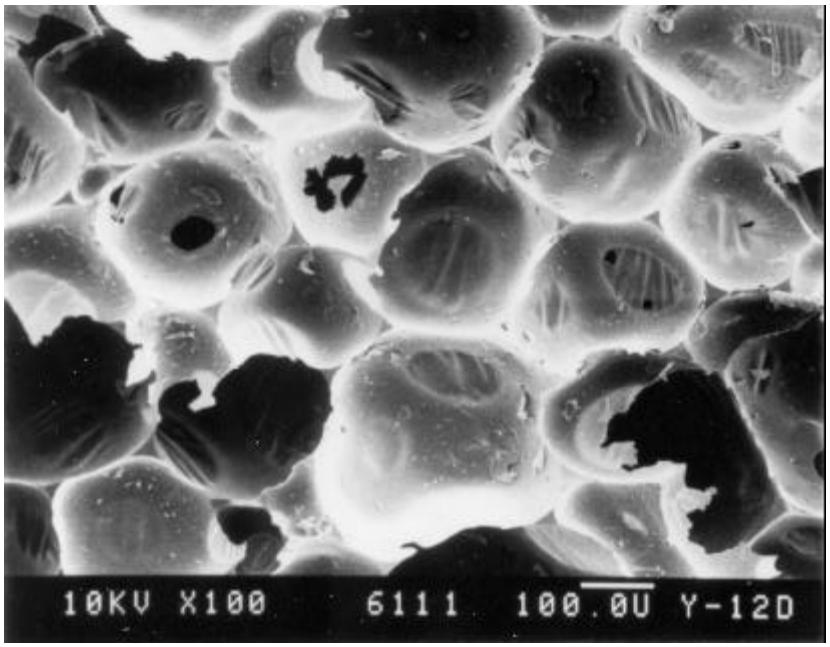

Figure 1. Glassy carbon foam structure made by Googin et al.

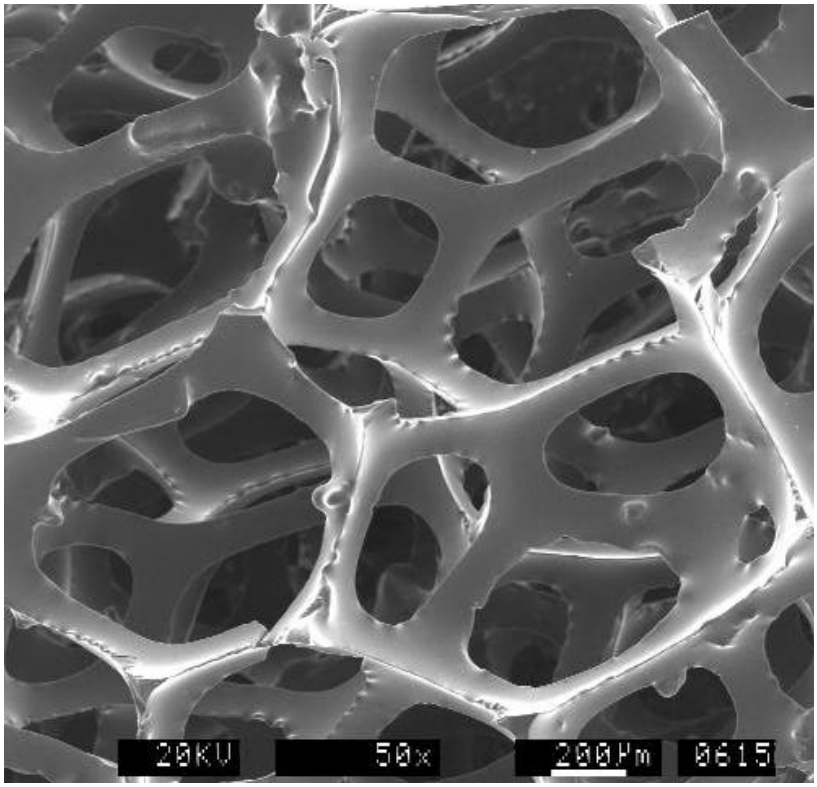

Figure 2. Reticulated foam structure (reticulated carbon foam made by ERG Corp.).

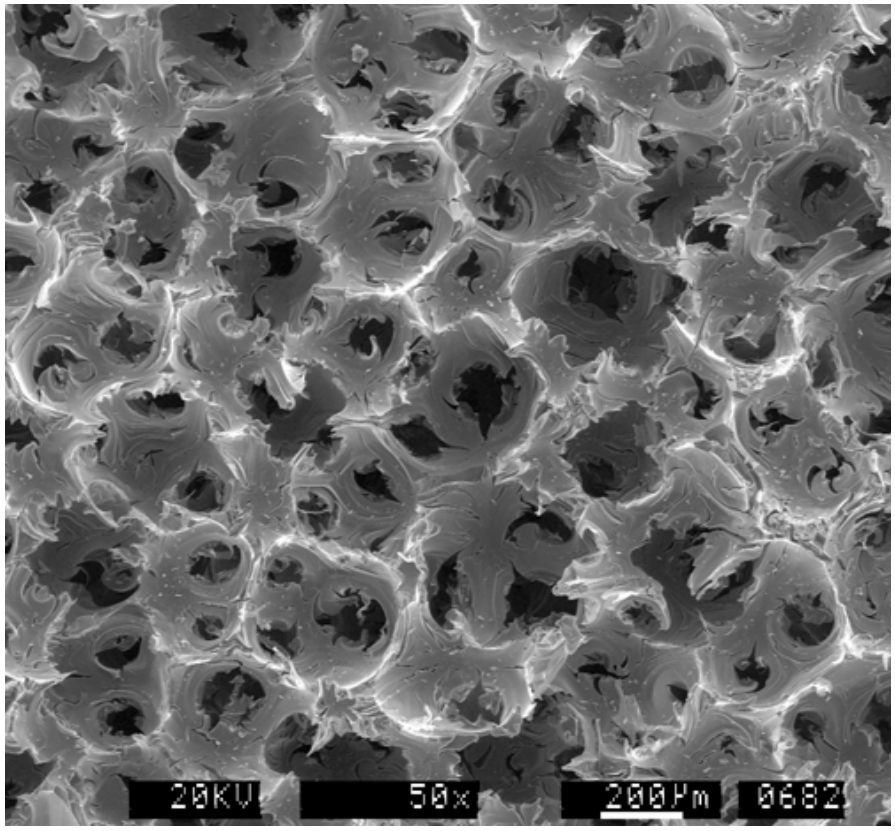

Figure 3. Spherical pore structure of pitch-based graphite foams by Klett (4).

A typical heat transfer configuration is shown in Figure 4. A heat source is bonded or joined to a thin conductive substrate on which a block of graphite foam of length L and thickness b is attached. The foam is then placed in a channel, and a cooling fluid of velocity V_f at a temperature T_i is pumped through the open celled material, thereby affecting heat transfer from the hot source to the cooling fluid. Many models for heat transfer for laminar fluid flow in a channel employ a constant Nusselt (N_{Nu}) number. This implies that the localized heat transfer coeffecient is independent of fluid velocity, and is valid for most cases of flow in a channel. However, in our case with flow through a porous medium, researchers (1, 2) have shown that the localized heat transfer coefficient will vary with velocity, even at local Reynolds number less than 50 (BSL). This is primarily due to a physical phenomena caused the tortuous nature of the porous flow. At the openings between the cells, where the fluid passes from one cell to another, the fluid passes through a contraction and expansion. At the back side of the opening (expansion side) the fluid develops eddies and vorticies. These vorticies will affect the mixing and local boundary layers, thereby affecting localized heat transfer from the cell walls to the fluid. Therefore, it is evident that a model of the convective heat transfer in the foam must account for velocity effects (Reynolds number) in the Nusselt number.

The model developed by Ashby et al. for reticulated metal foams regards the foam as a slight variant of the staggered bank of cylinders (Figure 5). The foam's relative density is $\tilde{r} = \rho/\rho_s$, where ρ is the bulk apparent density and ρ_s is the skeletal density. The diameter of the bubble is

d_p, the ligament diameter is d_l, and the local heat transfer coefficient at the surface of the walls is given by h_{loc}.

From these basic principles, we can begin to develop a model for heat transfer utilizing the graphite foam as the primary heat transfer medium. First, heat transfer from the foam to the fluid will increase as either the bubble diameter decreases (thus increasing surface area for heat transfer) or as the relative density increases (thus increasing heat conduction through the ligaments) or as the velocity of the fluid increases. However, all of these methods to increase heat transfer will result in increased pressure drop through the system. Thus, a delicate balancing act must be performed so as to maximize the ratio of heat output to pumping power.

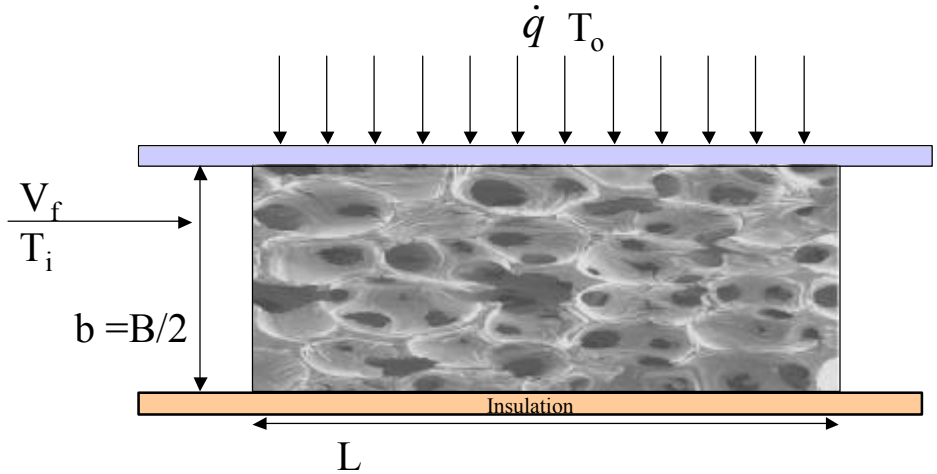

Figure 4. Schematic of heat transfer design as used with this model.

Heat Transfer Model

The thermally conductive graphite foam is a complex system that transfers heat from a hot source to a fluid by combining several unique characteristics. First, the extremely high ligament conductivity rapidly transfers the heat to all the surface area of the foam where it can then be transferred to the fluid. Next, the very large surface area provides for an efficient transfer of heat to the fluid.

In previous efforts to model heat transfer in reticulated metal foams (1) which are identical in structure to Figure 2, a staggered bank of cylinders was chosen as the model system (Figure 5) and the Biot number was used as the model for heat transfer. However, the assumption in this case is that the turbulence is governed by flow over cylinders and that the relative density is low, less than 0.1, (i.e. the gap between cylinders is much larger than the diameter of the cylinder). Unfortunately, in the current case with a spherical pore structure (Figure 3) and higher relative density, about 0.3, this fails to capture the essence of the fluid dynamics (compare Figure 2 to Figure 3). In the case of the graphite foam, the behavior of the system most resembles heat transfer through a packed bed and the Nusselt number is a good approximation of heat transfer within the pores (26).

This process, in which the heat is transferred to a fluid in the pore, is characterized by the localized heat transfer coefficient, h_{loc}, the fluid conductivity, k_f, and is related to the Nusselt number, N_{Nu}, as follows:

$$N_{Nu} = \frac{h_{loc} \cdot d_p}{k_f} \qquad \text{(Eq 1)}$$

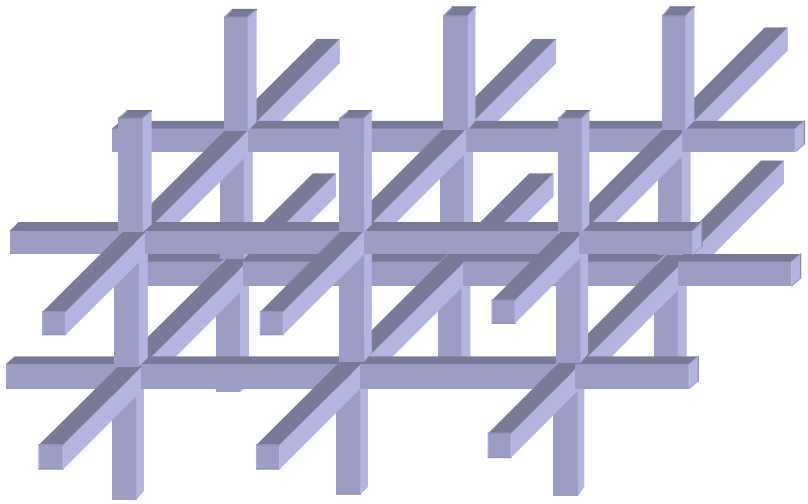

Figure 5. Staggered Bank of Cylinders

The heat transfer in the graphite foam model of this paper was then determined to be a function of Reynolds number in the same manner as Holman (28) and Ashby (1), except that the Biot number and ligament diameter in their model are replaced with the Nusselt number and the bubble diameter. This falls in line with standard relationships for heat transfer in packed beds (26). This relationship is also based on the foam properties and fluid constants as follows

$$N_{Nu} = m\, N_{\mathrm{Pr}}^{0.36}\, N_{\mathrm{Re}}^{\ y} \qquad \text{(Eq 2)}$$

Where

$$N_{\mathrm{Re}} = \frac{V_f d_p}{n_f} \text{ (Reynolds number),} \qquad \text{(Eq 3)}$$

and

N_{Pr} = Prantl number for the fluid (0.72 for air), and
d_p = bubble diameter and
n_f = kinematic viscosity of fluid, and
V_f = free stream velocity of fluid, and

m and y are experimentally determined constants fit to this material and are equal to:

m = 0.0158
y = 0.7225

It is important to note that these parameters were fit to graphite foam produced in the laboratory at ORNL. For a similar material fabricated with a slightly different process and exhibiting a slightly different structure, the parameters will be different.

This model is consistent with the system and provides a reliable representation for the heat transfer. For, example, according to the model, as the bubble diameter approaches the hydraulic diameter of the system (as the relative density approaches zero), the foam disappears and the Reynolds number approaches that for a fluid flowing through a channel.

Conversely, as the diameter decreases, the Reynolds number will decrease (as commonly seen with small tubes and microchannels), until the system actually becomes a closed foam and there is no fluid flow. In a more refined model, the diameter of the opening between the cells (or the web) will be included as a ratio to the diameter of the bubble (similar to that used in calculating frictional losses in entrances and exits to channels) (26).

Heat Fluxes

Typically, the overall heat transfer per unit width, Q, is then calculated in a standard fashion (BSL) as

$$Q = L \cdot h_{loc} \cdot A \cdot \Delta T \ , \qquad \text{(Eq 4)}$$

where L is the flow length, A is the overall surface area of heat transfer and ΔT is the temperature difference between the surface and the fluid and is the main driving force for heat transfer. Obviously, the goal of a heat exchanger system is to develop a system with the largest surface area, largest temperature difference, and the largest localized heat transfer coefficient to maximize the results. However, to model heat transfer in these foam materials, since it is unthinkable to measure an accurate surface area, the local heat transfer coefficient and the surface area are replaced with an effective overall heat transfer coefficient, h_{eff}, as such:

$$Q = L \cdot h_{eff} \cdot \Delta T \ , \qquad \text{(Eq 5)}$$

Typically, the ΔT is represented by the log mean temperature difference (ΔT_{LM}) between the hot source (T_h) and the inlet and exit fluid temperatures (T_i and T_e, respectively). This is given by

$$\Delta T_{LM} = \frac{T_e - T_i}{\ln\left(\dfrac{T_h - T_i}{T_h - T_e}\right)}, \qquad \text{(Eq 6)}$$

There have been many attempts to model heat transfer in foams. Ashby et. al showed that a staggered bank of cylinders gave good correlation to reticulated metal foams in the past. This model correlates the ligament diameter, the thickness of the foam, and the biot number (which incorporates by definition the ligament conductivity and the local heat transfer coefficient). However, as mentioned earlier, since our system with spherical pores behaves more like a packed bed, the ligament diameter in their model is replaced with the bubble diameter.

$$h_{eff} = \frac{2}{d_p}\tilde{k}\sqrt{N_{Nu}\left(\frac{k_f}{k_s}\right)}\tanh\left[\frac{4b}{d_p}\sqrt{N_{Nu}\left(\frac{k_f}{k_s}\right)}\right], \qquad \text{(Eq 7)}$$

where

k_f = thermal conductivity of fluid, and

k_s = thermal conductivity of solid ligament.

$\tilde{k}$ = bulk thermal conductivity of foam and is defined as

$$\tilde{k} = 0.35\left(\frac{r_{bulk}}{r_{ligament}}\right)k_s$$

The fluid temperature is governed by the following equation:

$$T_f = T_1 - (T_1 - T_0)\cdot e^{\left(\frac{-x}{l}\right)}, \qquad \text{(Eq 8)}$$

where l is a characteristic heat transfer length defined as

$$l = \frac{r_f C_{p,f} b V_f}{h_{eff}}. \qquad \text{(Eq 9)}$$

To compare the heat flux to other parameters, as is desired in a parametric study when optimizing heat transfer systems, it is best to represent the heat flux as a dimensionless quantity related to the fluid thermal capacity, i.e;

$$\tilde{Q} = \frac{Q}{r_f V_f L[T_1 - T_0]}. \qquad \text{(Eq 10)}$$

Pressure Drop and Pumping Power

Other parameters desired in the parametric study are the pressure drop and the power required to pump the fluid through the foam.

The pressure drop was determined by Ashby et. al and is governed by the general relation:

$$\frac{\Delta P}{L} = x\left(\frac{1}{a}\right)\left[\frac{-n_f^n r_f}{(1-a)^{2-n}}\right]V_f^{\,2-n} d_p^{\,-n}, \qquad \text{(Eq 11),}$$

where

$$a = 1.24 d_p \sqrt{\frac{3p}{\tilde{r}}}$$

$$a = \frac{n_f}{N_{\mathrm{Pr}}}.$$

The parameters ξ and n are determined through experimental fitting, and were estimated to be 0.0062 and 0.7668 respectively, for this material. From this, the pumping power is calculated by (26),

$$\tilde{P} = \frac{\Delta P}{L} \cdot L \cdot V_f \cdot A, \qquad \text{(Eq 12)},$$

where A is the cross sectional area of the foam in the flow direction.

Experimental Results

This model was validated using graphite foam in the test rig shown in Figures 6 and 7. Air was passed through the foam at various flow rates and heat was added to the system at various levels up to 600 watts (or 23 W/cm^2). The inlet and exit temperature of the air were monitored and the temperature of the base plate was measured. Last, the pressure drop across the foam at the various air flow rates was measured. Figure 8 shows the results of these tests.

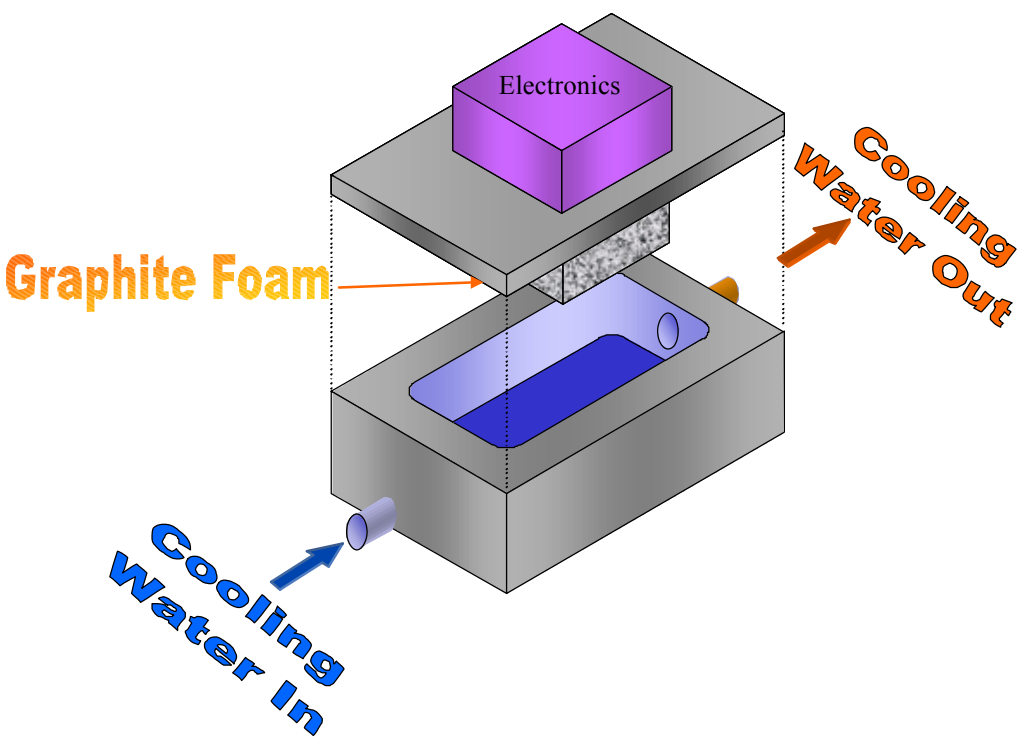

Figure 6. Schematic of test system to determine parameters of model.

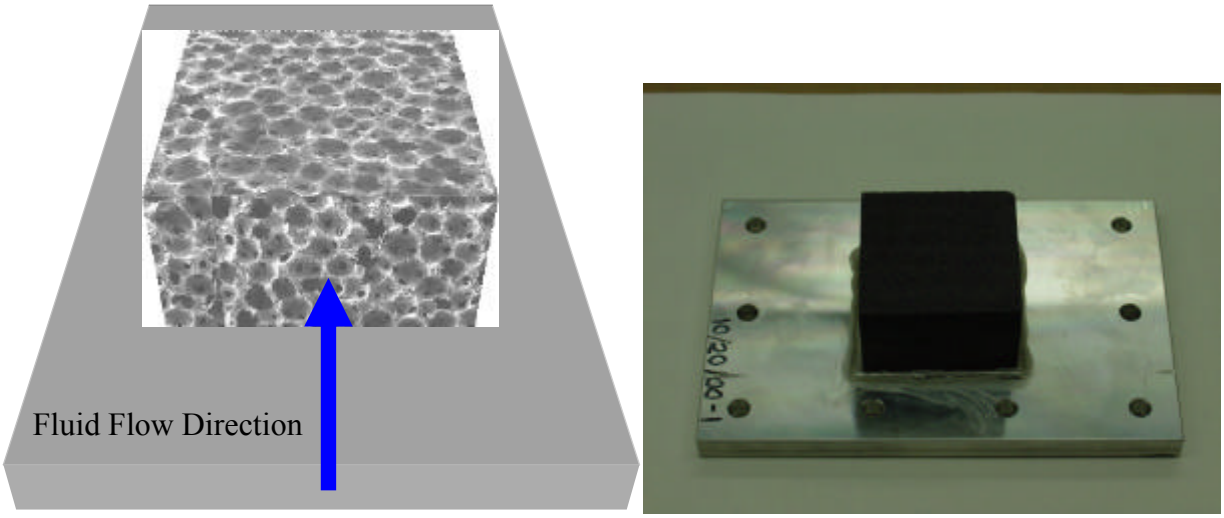

Figure 7. Figure of model heat sink and actual heat sink with foam.

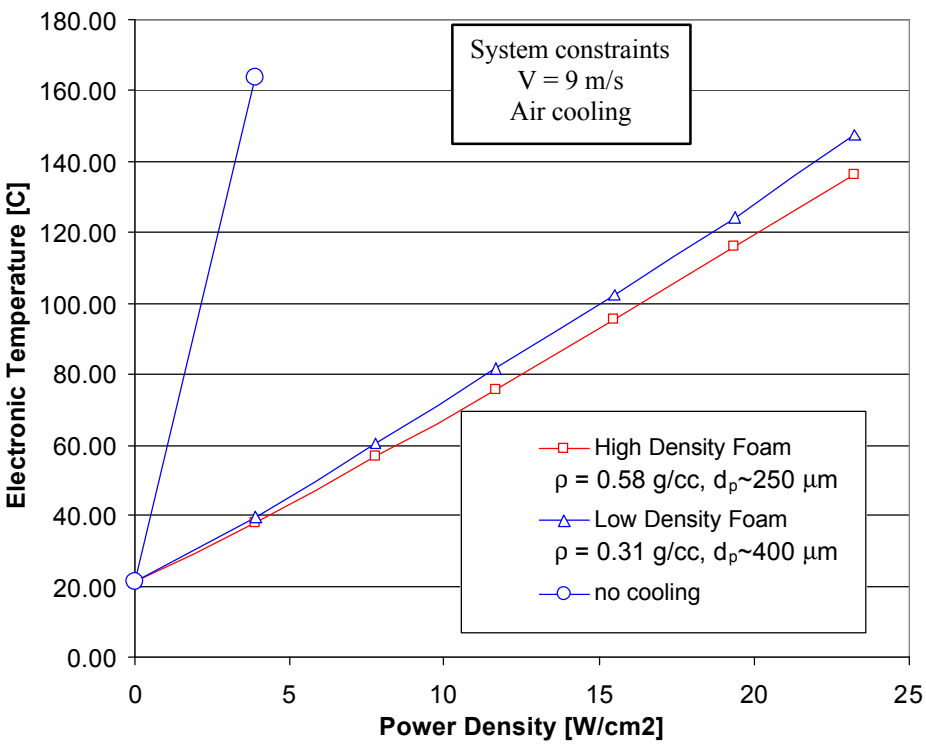

Figure 8. Heater temperatures versus power density at various flow rates of air for graphite foam heat sink. Note that this system is designed with a constant flux heat source, rather than a constant temperature heat source.

Model Results

With these experiments completed, this was then compared to the model in an attempt to optimize the system. The Nusselt number can be plotted as a function of bubble diameter and fluid velocity, Figure 9. This figure represents the ratio between the local heat transfer from the foam to the fluid and the thermal conductivity in the fluid (i.e. an effect of the spreading effect of the heat in the fluid). Clearly, a higher number is better, as the fluid thermal conductivity does not change with a change in the velocity, bubble size, geometric structure of the sink, etc. As expected, an increase in bubble diameter results in a linear increase in Nusselt number. As seen from equation 3, the Reynolds number is also directly dependent on the fluid velocity, with an increase in fluid velocity and bubble diameter increasing the Reynolds number. This is observed in the plot of the Reynolds number (Figure 10), indicating a reasonable representation of the model with the physics of the system. However, one can also notice that the effects of velocity on the Nusselt number are very limited at higher bubble diameters. This indicates that at higher bubble diameters (similar to packed beds and metal foams), the Nusselt number will be for the most part constant, and will match that of other models of porous media heat transfer which assume a constant Nusselt number with velocity.

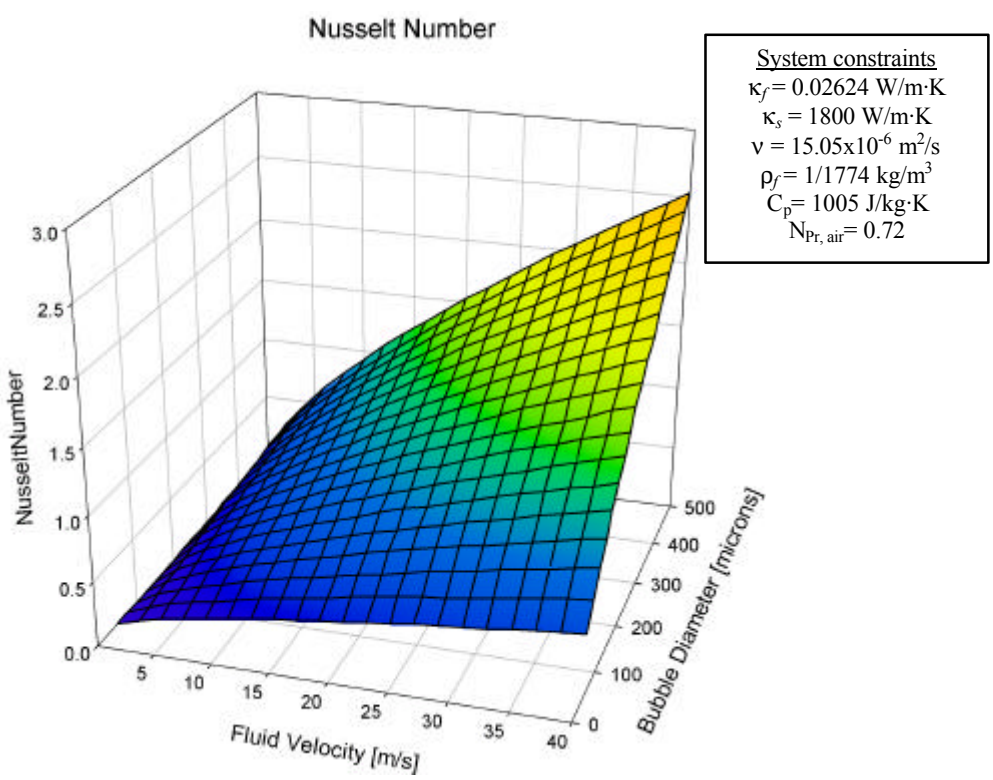

Figure 9. Plot of Nusselt number as a function of fluid velocity and bubble diameters in the foam.

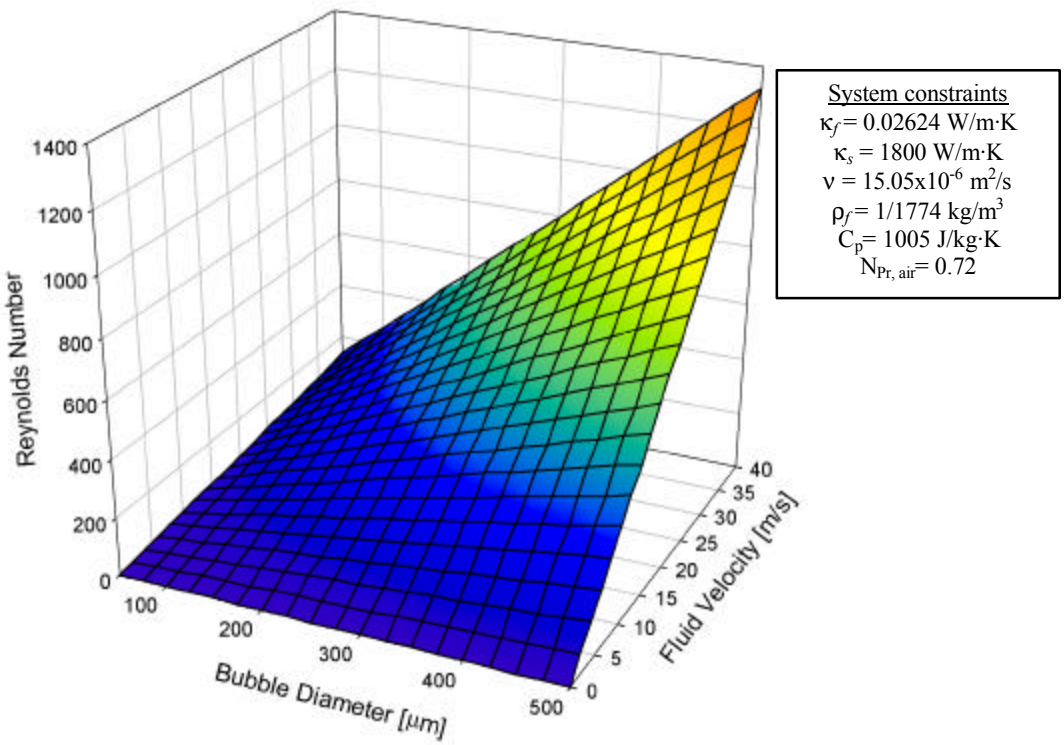

Figure 10. Local Reynolds Number versus bubble diameter and fluid velocity.

If we then plot the effective heat transfer coefficient, h_{eff}, as a function of the bubble diameter and the fluid velocity (Figure 11), we can gain an appreciation for which parameter has a larger effect on heat transfer. Clearly, this figure shows what is intuitive with the foams in this system. First, as the fluid velocity increases, it is intuitive that the heat transfer coefficient will increase because the Reynolds number will increase and improve mixing (this is observed in the plot). Also, it appears that this effect is more pronounced at smaller bubble diameters. However, it is not intuitive that the heat transfer will necessarily increase as the pore size decreases. As noted earlier, we observed that the Nusselt number decreased with decreasing bubble diameter, therefore we might anticipate that the heat transfer would be unaffected by the bubble diameter. However, it is also noted that the surface area available for heat transfer increases inversely with the square of the bubble diameter. Also, the Reynolds number changes with a change in bubble diameter, and hence a change in turbulence and mixing occurs. However, this is a linear effect. So, it would be anticipated that the surface area would be more dominant, and from the results in Figure 11, is appears that this is the case. Unfortunately, as we will discuss later, the pressure drop also increases dramatically as the bubble diameter decreases, and therefore the pumping power to force the fluid through the foam will increase dramatically. This pumping power will have to be balanced with the increase in heat transfer.

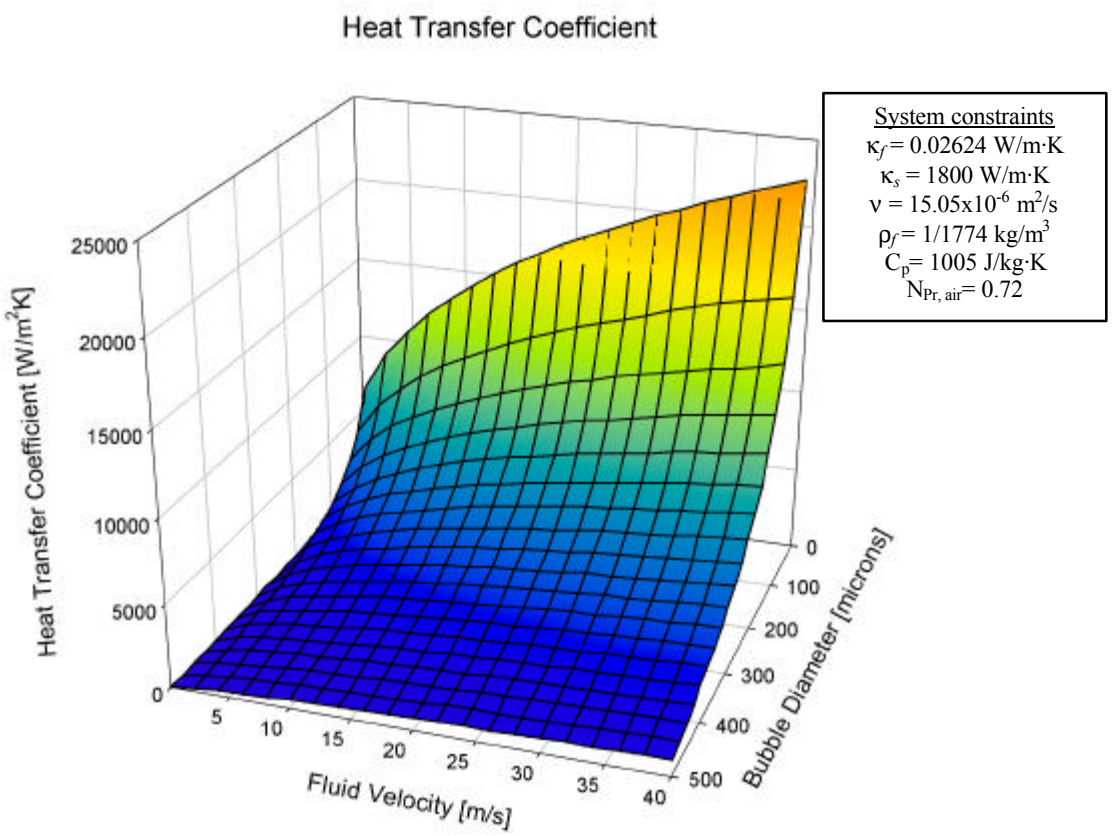

Figure 11. Plot of effective heat transfer coefficient as a function of fluid velocity and bubble diameters in the foam.

Next, with the model we can predict the temperature profiles and the exit temperature of the air (Figure 12) in the system. The temperature of the fluid is the driving force for heat transfer. The larger the temperature difference between the fluid and the heat source, the higher the heat flux and the more heat removed. This is a critical and difficult parameter to optimize. On one hand, you want the lowest average fluid temperature in the system (i.e. the lowest temperature rise of the fluid) to increase the driving force for heat transfer. However, this typically requires either a colder inlet temperature (which is usually not realistic) or higher fluid flow. A larger quantity of fluid results in an increase in fluid velocity, but also increases pressure drop with the square of the velocity. On the other hand, if you decrease the fluid flow to reduce the pressure drop, this typically results in a larger temperature rise across the system, and a lower average temperature difference, and unfortuntately a decrease in heat flow. It is a "catch-22" that engineers have been wrestling with for many years. As can be seen, increasing the velocity decreases the fluid temperature in the system. Also, a complimentary increase in bubble size reduces fluid temperature. However, these effects are due to a corresponding decrease in heat transfer due to reduced surface area as the bubble size increases. On the other hand, the velocity effect on heat transfer is simply due to the increase in heat capacity of the fluid flowing through the system, thus reducing the sensible heat change of the fluid. From these results, it is apparent that the optimum design would have the flow of the fluid flow normal to the base plate and out

the two ends of the system. This would optimize the heat transfer and is analogous to counter flow heat exchangers.

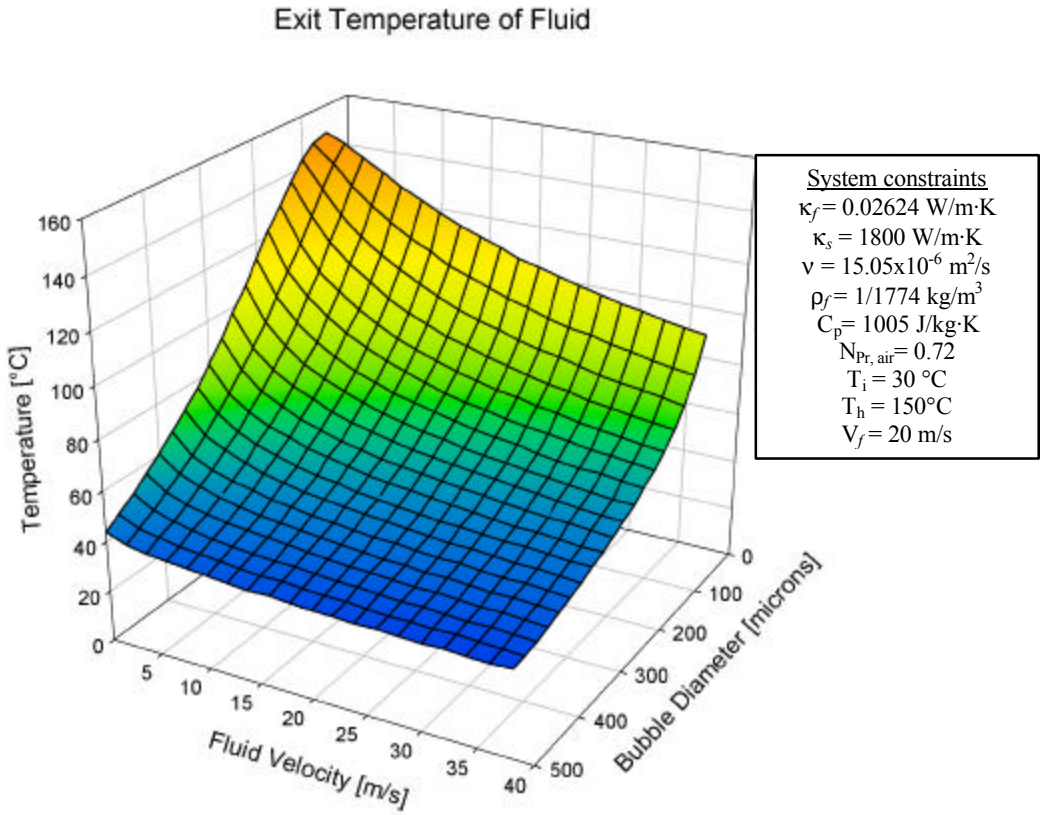

Figure 12. Plot of exit temperature as a function of fluid velocity and bubble diameters in the foam.

The heat flux is the real quantity that drives the final designs of most heat exchangers (other than cost and manufacturability). Simply put, people want to maximize the heat output in the smallest volume. This heat flux is usually represented as a dimensionless quantity, $\widetilde{Q}$, as previously discussed, and is plotted in Figure 13. It can be seen that an increase in the bubble diameter results in a corresponding reduction in the overall dimensionless heat flux, which is intuitive when observing the plot of heat transfer coefficient. However, it is noted that an increase in fluid velocity decreases the dimensionless heat flux. This is also intuitive as the dimensionless heat flux is the ratio of the heat flux to the thermal capacity of the fluid. As the fluid velocity increases, there is a smaller sensible heat change, and therefore the ratio is decreased, but overall heat transfer may be increased. It is also seen that this effect of velocity on heat transfer is more prominent as smaller bubble sizes. This may be a result of two effects. First, the smaller bubble size decreases turbulence, thereby decreasing heat transfer. However, a smaller bubble size increases the surface area by the square of the bubble diameter, therefore, this effect should be more significant. Second, as the velocity increases, the average fluid temperature decreases, thereby increasing the temperature difference and increasing heat transfer. However, again, this will have to be balanced with the pressure drop and overall pumping power.

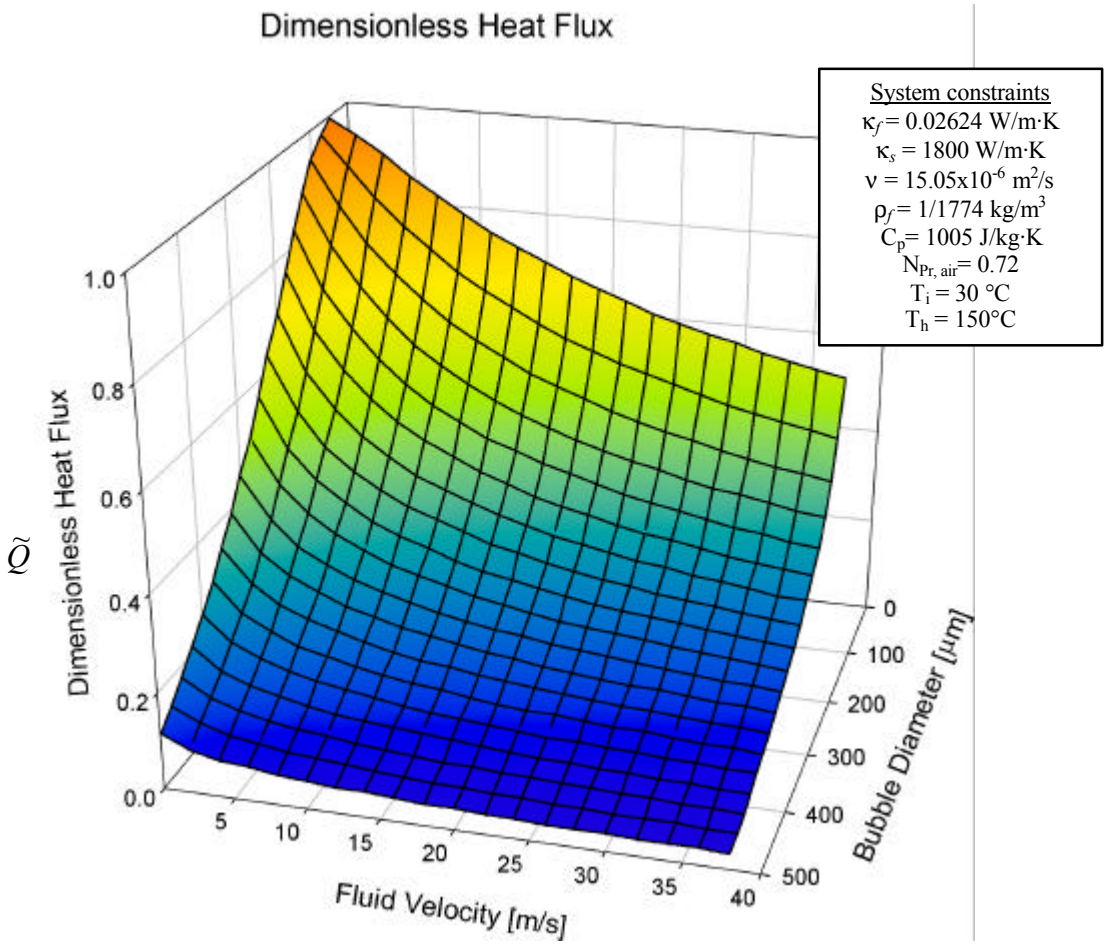

Figure 13. Plot of dimensionless heat flux as a function of fluid velocity and bubble diameters in the foam.

Now that the relative effects of velocity and foam structure are understood, it is important to determine optimum geometry of the system. The first, and easiest, parameter to model is the ratio of the thickness, b, of the foam to the length of the heat transfer section, L. If we plot the fluid exit temperature as a function of the fluid velocity and the relative thickness, b/L, we can ascertain that the relative thickness has a larger impact on the heat transfer than the fluid velocity. If we increase the thickness at a constant velocity, this will correspond to an increase in volumetric (or mass) flow. This excess heat capacity of the fluid is important in providing a lower working temperature and improved heat transfer. If we increase b/L at a constant volumetric flow rate, then the relative velocity will decrease, thereby increasing the temperature of the working fluid. For example, if a model with an inlet velocity of 40 m/s and a relative thickness of 0.2, and the system is compared to one with a relative thickness of 0.4, then the flow velocity decreases to 20 m/s. However, if this is plotted with the model, it is seen from Figure 14, that the end result is still a decrease in fluid exit temperature (a result of the fact that the relative thickness has a larger effect on improving heat transfer than the decrease in velocity has in decreasing heat transfer. It is anticipated that this is due to the extremely high thermal

conductivities of the cell walls of the graphite foam. If the foam exhibited thermal conductivities similar to metal foams (i.e. 10x less), this effect would be minimized.

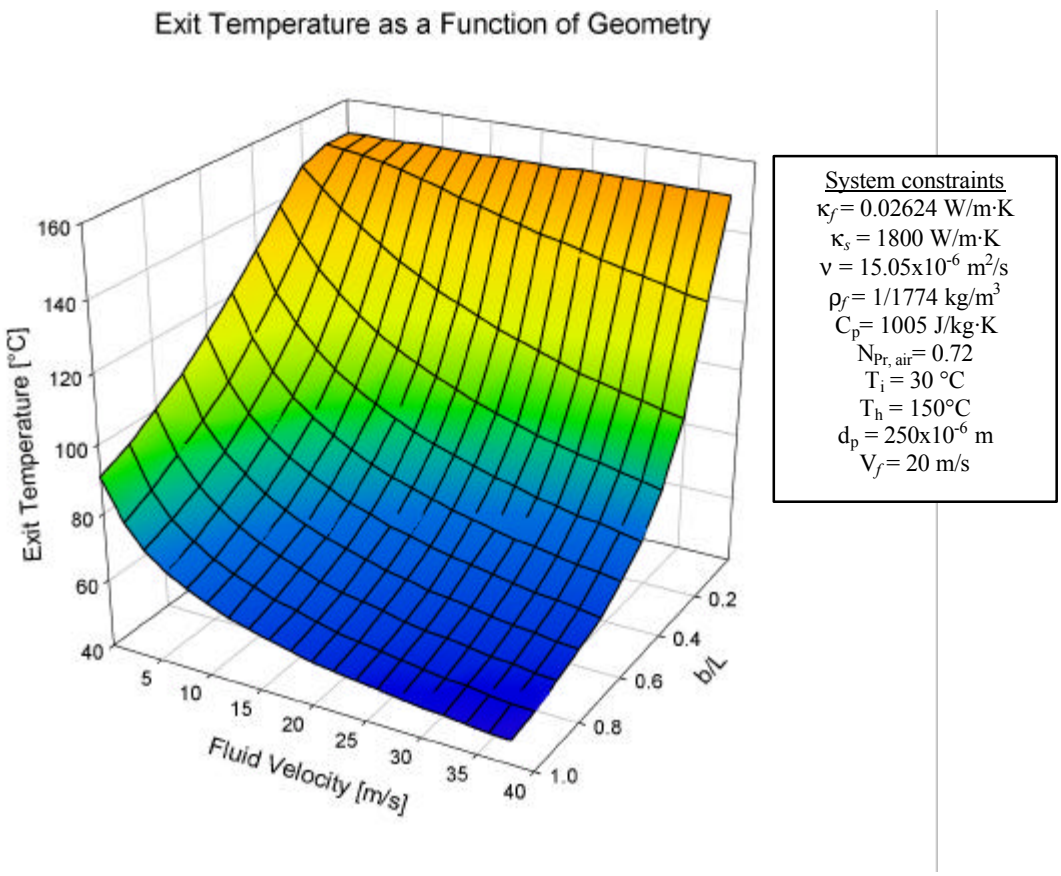

Figure 14. Plot of exit temperature as a function of fluid velocity and relative foam thickness.

Next, we can plot the effect of the system geometry on the overall dimensionless heat flux (Figure 15). First, as the fluid velocity increases, the overall dimensionless heat flux decreases. Again, this is simply that there is less sensible heat change of the fluid and a larger thermal capacity due to the higher velocities. As the relative thickness increases, the overall flux also increases. At a constant fluid velocity, an increase in relative thickness increases the volumetric flow (with a corresponding increase in thermal capacity of fluid and lower temperatures), thereby increasing heat transfer. At a constant volumetric heat flow, an increase in b/L results in a decrease in velocity, with a corresponding decrease in turbulence and heat transfer. However, it is shown that at high velocities, there is a rapid limit to the benefits in increasing relative thickness. However, at low velocities, it appears that the effects of relative thickenss on heat transfer are more pronounced. This is a very important result of this model. Simply put, it does pay to reduce velocity by increasing the relative thickness. This also will pay off in that a decrease in velocity by a factor of 2 will decrease the pressure drop by a factor of about 4. Hence, we have found a method to possibly increase heat transfer while reducing pressure drop.

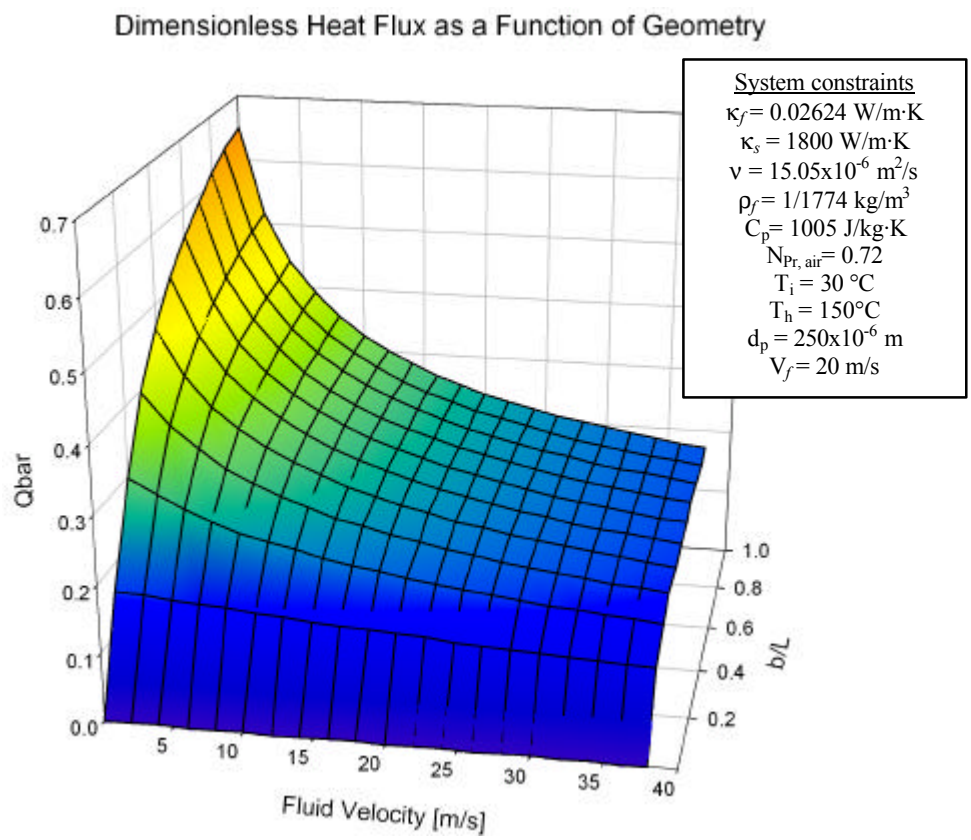

Figure 15. Plot of dimensionless heat flux as a function of fluid velocity and relative thickness of the foam.

As mentioned earlier, the balance between heat transfer and pressure is critical to developing a system which is commercially viable. Therefore, it is important to plot the power required to pump the fluid through the system versus the system parameters, (see Figure 16). This is a relatively intuitive plot which shows that the fluid velocity affects the pumping power dramatically, but mostly at the smaller bubble sizes. It appears that at larger pore diameters, the effect of fluid velocity will not affect the power requirements that significantly. However, it may be more representative to plot the ratio of dimensionless heat flux to the pumping power versus the system parameters (Figure 17). It can be seen that there is a maximum of heat transfer for the pumping power required at a bubble size of about 450 microns. It is also noted that reducing the fluid velocity also increases the heat transfer to pumping power ratio. Therefore, it appears that a system which accommodates low fluid velocities (preferably by increasing the b/L ratio) and bubble diameters in the range of about 450 microns, would provide the optimum heat transfer. However, this does not mean that this is the optimum design for maximum heat transfer. The design for maximum heat transfer will clearly be different.

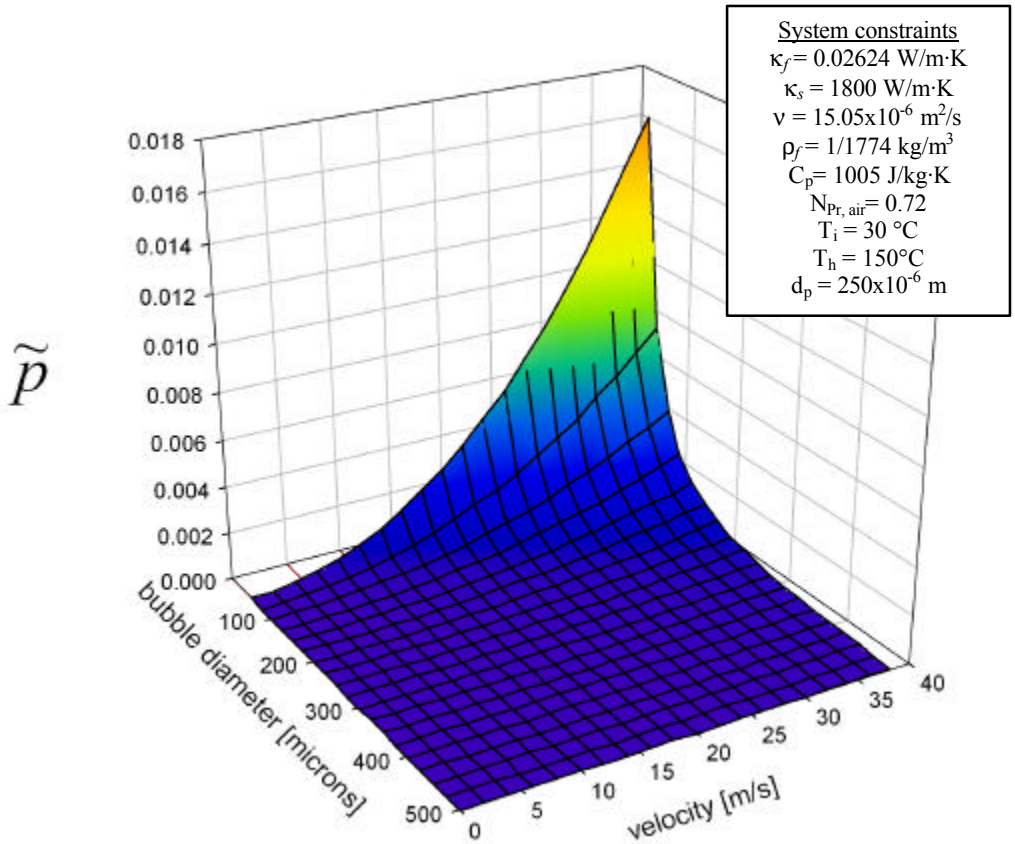

Figure 16. Plot of pumping power as a function of fluid velocity and bubble diameters.

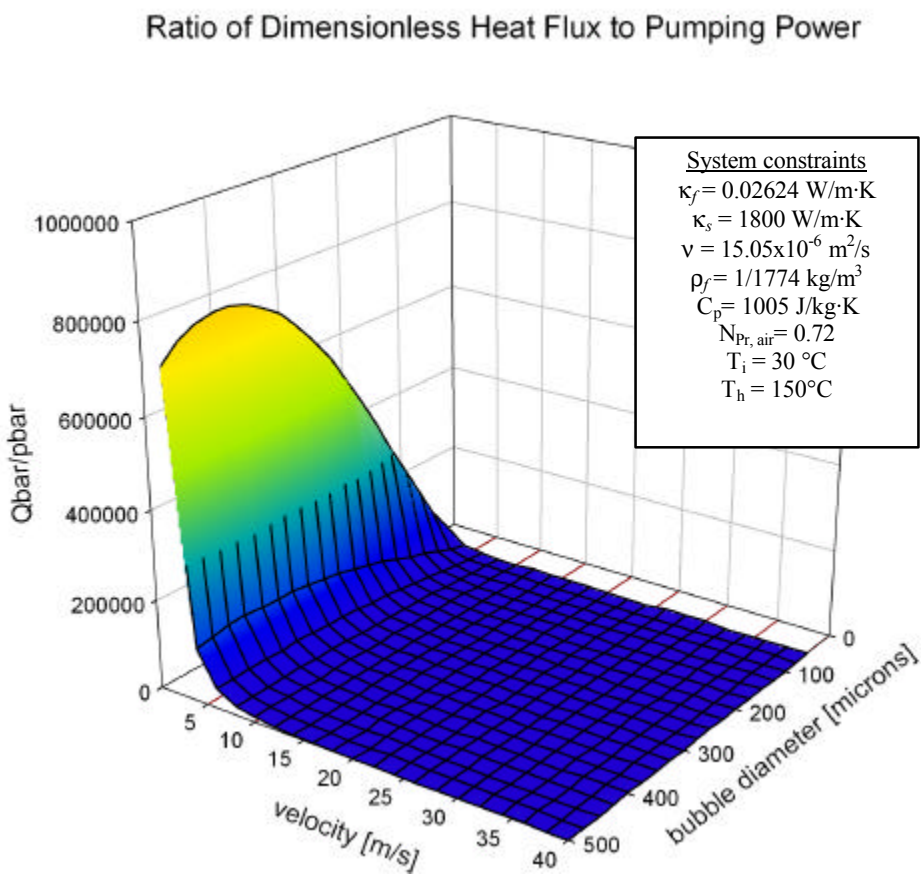

Figure 17. Plot of ratio of dimensionless heat flux to pumping power as a function of fluid velocity and bubble diameter.

Another method to study the parameterization of the system is to plot the pumping power directly versus the inverse of the dimensionless heat flux. This is shown in Figure 18. As seen, a corresponding increase in pumping power results in a decrease in heat flux for a given pore diameter. Also, a decrease in bubble size shows an increase in heat flux for a constant pumping power (a shift in the curve to the left). However, the slope (or rate of decrease) changes as the pore diameter decreases. At some point, when the system reaches the thermal capacity of the fluid, any further decrease in pore diameter just increases the pumping power without affecting the heat flux. Therefore, it is evident that there is a optimum pore diameter which the foam should exhibit. If the pores get larger, the heat flux decreases and if they get smaller, the pumping power (pressure drop) gets bigger. This is the struggle with heat transfer that engineers have coped with for years.

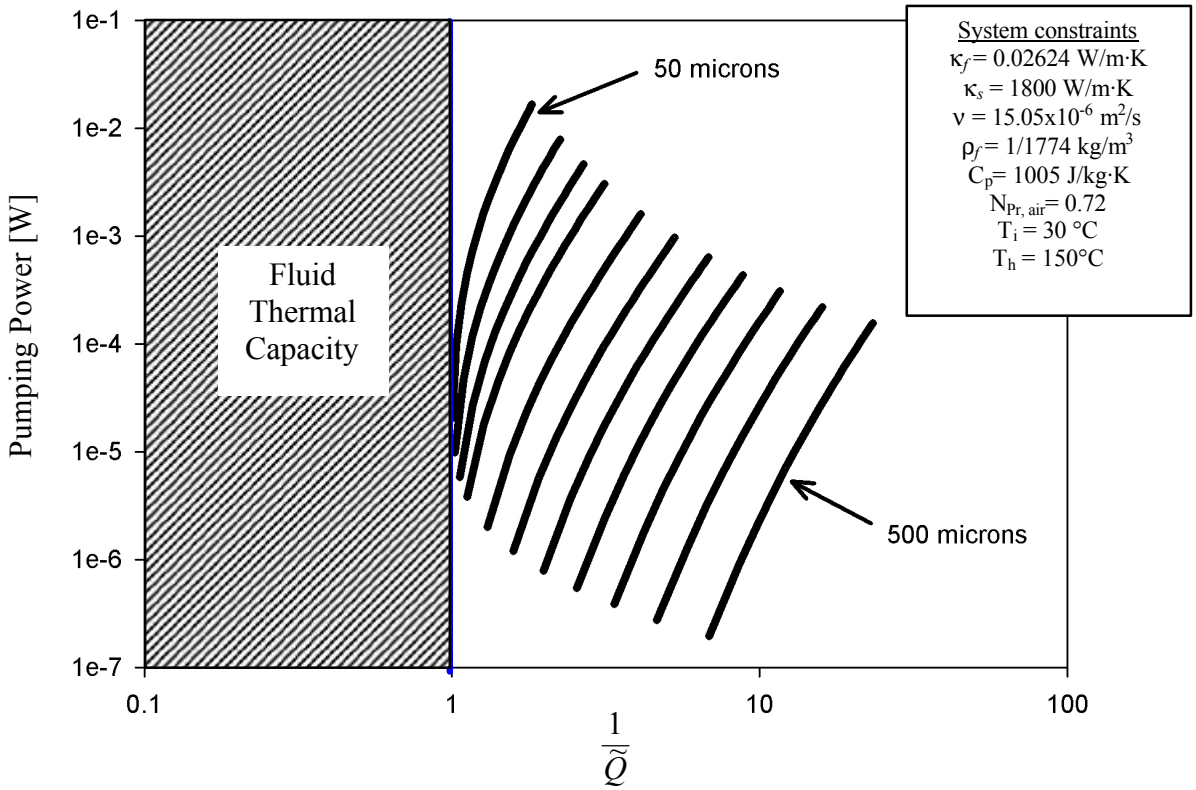

Figure 18. Plot of Pumping power versus inverse dimensionless heat flux.

So, in our earlier described system, a solid block of foam with thermal conductivity about 150 W/mK, relative density of 0.3, and an average pore diameter of 250 microns, we wished to improve heat transfer or reduce pressure drop. As seen earlier, if we increase the length to thickness ratio, the pumping power will drop while increasing heat transfer. However, the caveat is to not change the overall system geometry. This can be accomplished by corrugating the foam in the direction parallel to the fluid flow (see Figure 19). As with HEPA filters, which have sub-micron pores, corrugation is used to reduce pressure drop without sacrificing surface area. The concept for heat transfer is to reduce the flow path (increase the thickness to flow length ratio) while maintaining the contact with the hot source. This was tested and the results are shown in Figure 20. As can be seen, the pressure drop decreased to a point which was not measurable on the gauges for the current system which the overall heat transfer was only slightly affected. This is an incredible result as by modifying the system geometry with simple corrugation, the pumping power can be reduced dramatically without sacrificing heat transfer.

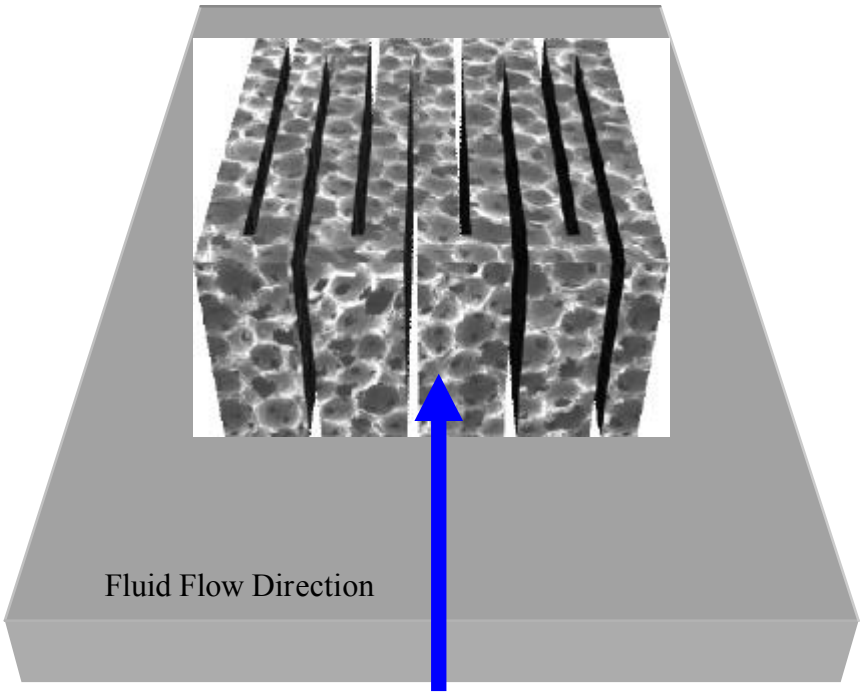

Figure 19. Slotted foam to reduce pressure drop and pumping power required.

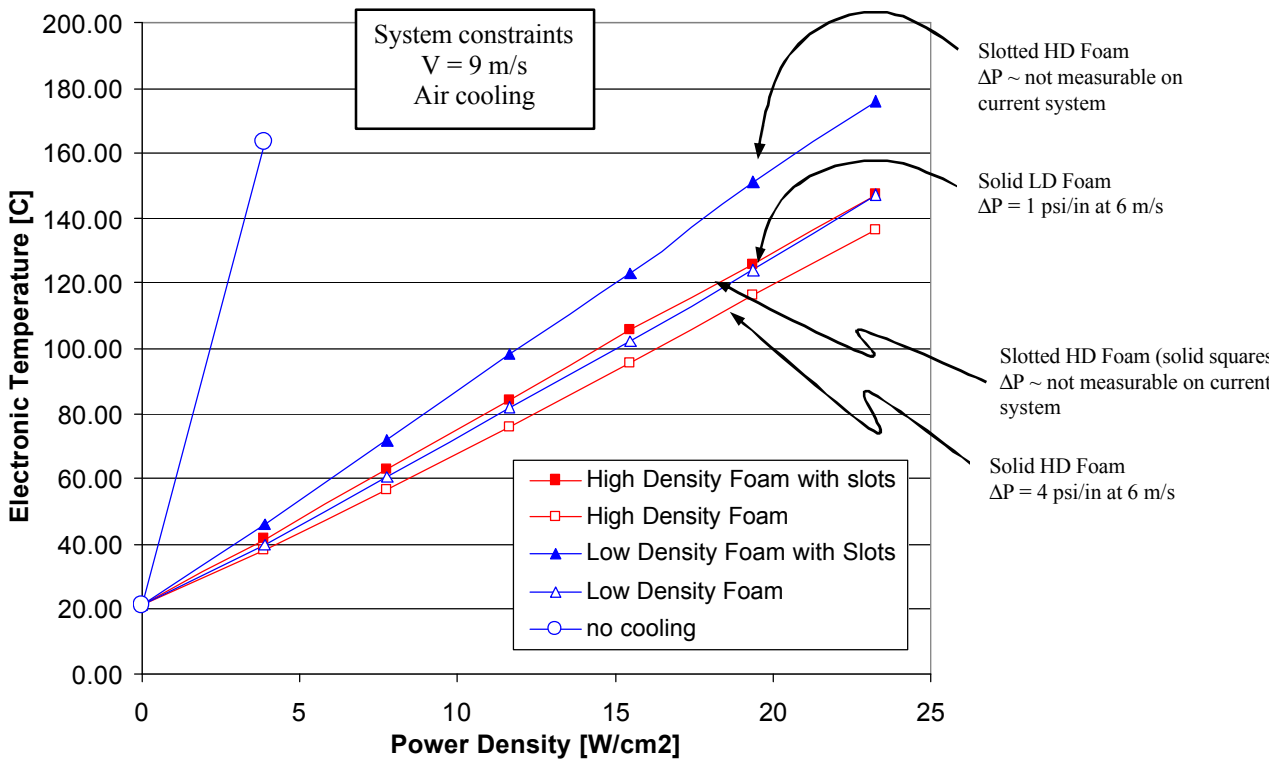

Figure 20. Results of slotted foam versus solid foam.

Conclusions

A model for the heat transfer with graphite foams was developed and presented. This model assumed heat transfer was dominated by the heat transfer of the fluid in the pores of the foam, rather than in the ligaments. In other words, since the foam is extremely conductive, the largest thermal resistance is at the local surfaces, rather than transmitting the heat through the foams (as is the case with metal foams). This model demonstrates several guiding principles of designing heat transfer devices utilizing cooling fluids and foams (1).

1. The highest conductivity ligaments are needed to transport the heat from the heat source rapidly into the foam so that it can then be transferred more uniformly to the cooling fluid.
2. While a turbulent fluid flow is desired to facilitate better mixing and high local heat transfer coefficients from the solid surfaces (ligaments) into the fluid, the effects of surface area are dominating as the surface area increases with the square of the change in bubble diameter and the Reynolds number (turbulence) decreases monotonically with the change in diameter.
3. A low pressure-drop of the fluid through the foam is desired so that the required pumping power does not become cumbersome. Hence, low fluid viscosities are desired.
4. It is necessary to model the heat transfer of a system with a parametric study to optimize the various variables on the heat transfer.

It was shown that there is a maximum pore diameter to optimize the ratio of dimensionless heat flux to pumping power. It was also shown that proper use of models could help optimize foam-based heat exchangers through parametric studies. For example, it was shown how the model could predict the effects of a geometric change in the system on reducing pressure while maintaining high heat transfer. This type of model should be very useful in developing revolutionary new and exciting heat transfer devices.

Acknowledgements
The authors wish to thank Materials Resources International for supplying the bonding process for attaching the graphite foam to the aluminum base plates.

Research sponsored by the U.S. Department of Energy, Assistant Secretary for Energy Efficiency and Renewable Energy, Office of Transportation Technologies, as part of the Fuel Cell for Transportation Program, under contract DE-AC05-00OR22725 with UT-Battelle, LLC.

References

1. Ashby, et al., “Metal Foams: A design Guide,” Chapter 13, “Thermal Management and Heat Transfer,” Butterworth-Heinemann, (2000).
2. Antohe et al. 1996
3. Kaviany, 1985

4. James Klett, Rommie Hardy, Ernie Romine, Claudia Walls , Tim Burchell, "High-Thermal-Conductivity, Mesophase-Pitch-Derived Carbon Foams: Effect of Precursor on Structure and Properties," *Carbon*, **38**(7), pp. 953-973 (2000).

5. James Klett, April McMillan, Ron Ott "Heat Exchangers for Heavy Vehicles Utilizing High Thermal Conductivity Graphite Foams," ," Proceedings of the Society of Automotive Engineering Government/Industry Meeting, June 19-21, 2000, Renaissance Hotel, Washington, D.C., USA.

6. James Klett, Lynn Klett, Tim Burchell, Claudia Walls, "Graphitic Foam Thermal Management Materials for Electronic Packaging, Proceedings of the Society of Automotive Engineering Future Car Congress, Crystal City, Washington, DC, April 2-6, 2000.

7. James Klett, Bret Conway, "Thermal Management Solutions Utilizing High Thermal Conductivity Graphite Foams," Proceedings of the 45th International SAMPE Symposium and Exhibition, Long Beach, CA, May 21-25, 2000.

8. James Klett, "High Thermal Conductivity Mesophase Pitch-Derived Graphitic Foams," Composites in Manufacturing, Vol 14, no. 4, 1999.

9. Ford, Walter, US Patent 3,121,050, "Method of Making Cellular Refractory Thermal insulating Material," (1964) (filed 1960).

10. Googin, John, and John Napier and Michael Scrivner, US Patent 3,345,440, "Method for Manufacturing Foam Carbon Products," (1967) (filed 1965).

11. Ettinger, Bruce, and Samuel Wolosin, US Patent 3,666,526, "Refractory Porous Bodies," (1972) (filed 1966).

12. Cowlard, F.C. and J.C. Lewis, "Vitreous Carbon--A New Form of Carbon," J. of Mat. Sci. 2:507-512 (1967).

13. Noda, T., M. Inagaki and S. Yamada, "Glass-like Carbons," J. of Non-Crystalline Solids, 1:285-302 (1969).

14. Knippenberg, W.F. and B. Lersmacher, "Carbon Foam," Phillips Tech. Rev., pp. 93-103 (1976).

15. Frank, H-G, et al., US Patent 3,784,487 "Process for Making a foam from a composition comprising bituminous masses, a novalac, and hexamethylenetratramine," (1974).

16. Klett, R, US Patent 3,914,392 "High Temperature Insulating Material," (1975).

17. Luhleich, Hartmut, et al., US Patent 3,927,187 "Method of Making Carbonaceous Bodies," (1975).

18. Marek, Ronald, and William Udichak, US Patent 3,922,334 "Foam Carbonization and Resulting Structure," (1975).

19. Vinton, Clarence, and Charles Franklin, US Patent 3,927,186 "Method for the Preparation of Carbon Structures," (1975).

20. Bonzom, Albert, et al. "Process for preparing pitch foams and products so produced," (1981).

21. Hager, Joseph W., "Idealized Strut Geometries for Open-Celled Foams," Mat. Res. Soc. Symp., Materials Research Society, 270:41-46 (1992)

22. Sandhu, S.S. and J.W. Hager, "Formulation of a Mathematical Process Model Process Model for the Foaming of a Mesophase Carbon Precursor," Mat. Res. Soc. Symp., Materials Research Society, 270:35-40 (1992).

23. Hagar, Joseph W. and Max L. Lake, "novel Hybrid Composites Based on Carbon Foams," Mat. Res. Soc. Symp., Materials Research Society, 270:29-34 (1992)

24. Klett, J., US Patent 6,033,506 “Process for making carbon foam,” (2000) (filed 1997)

25. Klett, J., US Patent 6,261,485 “Pitch-based carbon foam and composites,” (2001).

26. Kearns, K., US Patent 5,961,814, “Pitch Foam Composites,” (1999).

27. Kearns, K., US Patent 5,868,974, “Process for preparing pitch foams,” (1999).

28. Abrams, Frances L., Hager, Joseph W., Hall, Richard B., US Patent 5,770,127, “Carbon or graphite foam reinforced composites,” (1998).

29. Stiller; Alfred H, Stansberry; Peter G., Zondlo; John W., US Patent 6,346,226, “Method of making a carbon foam material and resultant product,” (1999).

30. Stiller; Alfred H, Stansberry; Peter G., Zondlo; John W., US Patent 6,241,957, “Method of making a carbon foam material and resultant product,” (2001).

31. Stiller; Alfred H, Yocum, Plucinski; Januz, US Patent 6,183,854 , “Method of making a reinforced carbon foam material and related product,” (1999).

32. Stiller; Alfred H, Stansberry; Peter G., Zondlo; John W., US Patent 5,888,469, “Method of making a carbon foam material and resultant product,” (1999).

33.

34. McCabe, Smith, and Harriet

35. Bird, Stuart, and Lightfoot.

36. Holman (1989)